ATL-COM-PHYS-2001-033
October 2, 2002

# Impact of Energy and Luminosity upgrades at LHC on the Physics program of ATLAS

**G. Azuelos[a], D. Benchekroun[b], O. Çakır[c], E. Elfgren[a], F. Gianotti[d], J.-B. Hansen[d], , I. Hinchliffe[e], M. Hohlfeld[f], K. Jakobs[f], C. Leroy[a], R. Mehdiyev[a,k], F.E. Paige[g], G. Polesello[h], H. Stenzel[i], S. Tapprogge[j], Z. Usubov[k,l], L. Vacavant[e]**

[a] *U. of Montreal, Montreal, Canada*
[b] *U. Hassan II Casablanca-Maarif, Casablanca. Morocco*
[c] *U. of Ankara, Turkey*
[d] *CERN, Geneva, Switzerland*
[e] *Lawrence Berkeley National Laboratory, Berkeley, CA*
[f] *Institut fur Physik, Johannes Gutenberg-Univeritat Mainz, Germany*
[g] *Brookhaven National Laboratory, Upton, NY*
[h] *INFN, Sezione di Pavia, Pavia, Italy*
[i] *Max-Planck-Institut fur Physik, Munich, Germany*
[j] *HIP, Helsinki, Finland*
[k] *Institute of Physics, Academy of Sciences of Azerbaijan, Baku, Azerbaijan*
[l] *Joint Institute for Nuclear Research, Dubna, Russia*

**Abstract**

The impact on the physics capabilities of the ATLAS detector of possible LHC upgrades is discussed. As a benchmark, an increase in the luminosity by a factor of ten is considered. For comparison, a doubling of the LHC energy is also explored. Both upgrades significantly enhance the physics capabilities of ATLAS. As measured in terms of the mass reach for new particles, the energy upgrade is more powerful. However, in cases where the effect of an upgrade is to increase the precision of measurements as a result of the larger data samples, the luminosity upgrade can be at least as powerful. The pile-up of minimum bias events at higher luminosity could limit the physics performance of ATLAS in areas where tagging of forward jets is needed.

# 1 Introduction

It is useful to consider the possible impact on physics of upgrades to the LHC which would permit operation at a higher luminosity. For comparison purposes, the effect of an energy increase will also be considered. Four basic scenarios for high energy/luminosity *pp* colliders are used in this note. The higher luminosity operation would correspond to a bunch spacing of 12.5 ns.

- A The approved LHC, *i.e.* $\sqrt{s} = 14$ TeV and luminosity of $10^{34}$ cm$^{-2}$ sec$^{-1}$
- B $\sqrt{s} = 14$ TeV and luminosity of $10^{35}$ cm$^{-2}$ sec$^{-1}$
- C $\sqrt{s} = 28$ TeV and luminosity of $10^{34}$ cm$^{-2}$ sec$^{-1}$
- D $\sqrt{s} = 28$ TeV and luminosity of $10^{35}$ cm$^{-2}$ sec$^{-1}$

Note that, while scenario B represents a realistic upgrade scenario for the LHC, scenarios C and D are much more speculative. The impact of the upgrades on detector performance has not been assessed in detail but a few general remarks are appropriate. The baseline performance is documented in [1]. The higher luminosity has a severe impact. In the case of the ATLAS Inner Detector, the Transition Radiation Detector would need to be replaced due to the high occupancy. Radiation damage would imply replacement or removal of the pixels and some of the silicon layers. Removal would imply loss of tracking, electron identification and b-tagging capability. Calorimeter performance is not expected to be impacted significantly in the central region; some of the Tile Calorimeters' scintillating fibers may need to be replaced. The forward calorimeter (FCAL) could suffer from space-charge effects. More shielding will be required for the forward muon system which will reduce the fiducial region. The reduced bunch spacing at very high luminosity could have a severe impact on the front-end electronics, trigger and DAQ components. For example, the front end pipeline buffers would be incompatible with the latency needed for the level-1 trigger. The level-1 muon trigger could also be compromised by increased occupancy in the Resistive Plate and Thin Gap Chambers.

The ATLAS B-physics programme [1] does not benefit significantly from the energy or luminosity upgrades. The programme is accomplished primarily at low luminosity and, as the total B cross section increases only slightly at the higher energy, the energy upgrade will have little impact. Similarly the top production rate is very large in the baseline LHC and, possibly apart from rare decay modes, the physics will be fully exploited at design energy/luminosity.

Physics processes involving the production of high-mass systems have cross-sections that rise rapidly with energy. While the luminosity upgrade has the capability to significantly enhance the LHC capability, one should expect therefore that, if the impact of upgrades is assessed in terms of mass reach for new particles, the energy upgrade will be more powerful. For cases involving somewhat smaller masses, the luminosity upgrade could be more powerful *provided that the detector performance can be maintained.* In subsequent sections, various high $p_T$ physics cases are studied ranging from QCD to extra-dimensions. Finally some conclusions are drawn.

# 2 QCD studies and searches for compositeness

For QCD studies at an upgraded LHC, a comparison of the reach in jet transverse momenta was carried out using a NLO calculation of the inclusive jet cross section [2]. The expected number of events with a jet above a transverse energy threshold is shown in Figure 1. Requiring that there be 1000 events above a threshold, the accessible $E_T$ is shown in Table 1. This comparison clearly

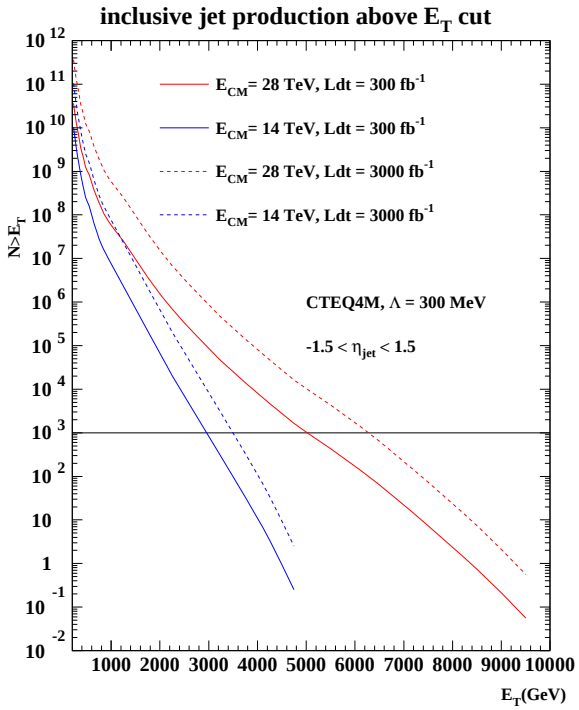


Figure 1: Expected number of events with a jet of transverse energy larger than $E_T$ for the four scenarios studied.

shows the advantage of increasing the center-of-mass energy to 28 TeV over a 10-fold increase in luminosity. In the former case, the reach extends by about 2 TeV, larger by a factor of four than in the latter case. As the measurements involve the calorimeters only and only jets in the TeV range are of interest, the detector performance is not expected to be degraded significantly at the highest luminosity.

Signals for quark compositeness should reveal themselves in deviations of the high energy part of the jet cross-section from the QCD expectation. The angular distribution of dijet pairs of large invariant mass provides an independent diagnostic and is less sensitive to possible non-linearities in the calorimeter response (see Section 21.5 of Ref [1] for more details on the methodology). It was therefore used in this study. Figure 2 shows the distribution for dijet events in the variable $\chi = (1+|\cos\theta|)/(1-|\cos\theta|)$, where $\theta$ is the angle between a jet and the beam in the center-of-mass frame of the dijet system. The invariant mass of the dijet system is required to be more than 10.5 TeV. Shown is the deviation from the expected form in the Standard Model for various values of the compositeness scale $\Lambda$ at $\sqrt{s} = 28$ TeV. The effect of compositeness shows up as an increase in the event rate at small values of $\chi$. The compositeness scales that can be probed in this manner are shown in Table 2. As this comparison of the scenarios is based on the production of the very highest energy particles, the energy upgrade more sensitive.

## 3 Higgs Boson studies

The Higgs physics discovery program will largely be completed before any upgrade. Following the discovery, the measurement of the mass will have reached the systematic limit, whereas measure-

| scenario | 14 TeV 300 fb$^{-1}$ | 14 TeV 3000 fb$^{-1}$ | 28 TeV 300 fb$^{-1}$ | 28 TeV 3000 fb$^{-1}$ |
|---|---|---|---|---|
| max $E_T$ (TeV) | 3.0 | 3.5 | 5.0 | 6.3 |

Table 1: The maximum value of jet transverse momentum that is accessible in various LHC energy/luminosity scenarios. The criterion is that there be 1000 events with $p_T$ greater than the value shown.

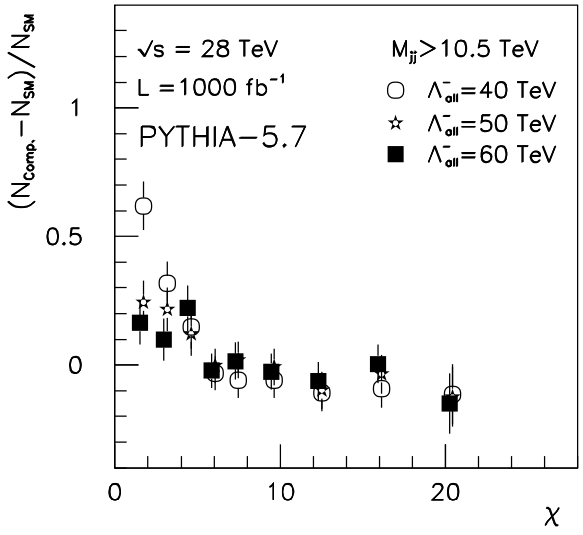


Figure 2: Expected deviation from the Standard Model predictions for the angular distribution of dijet pairs at 28 TeV for various values of the compositeness scale $\Lambda$. Dijet pairs are required to have invariant mass greater than 10.5 TeV.

| scenario | 14 TeV 300 fb$^{-1}$ | 14 TeV 3000 fb$^{-1}$ | 28 TeV 300 fb$^{-1}$ | 28 TeV 3000 fb$^{-1}$ |
|---|---|---|---|---|
| $\Lambda$(TeV) | 40 | 60 | 60 | 85 |

Table 2: The 95% confidence level limits that can be obtained on the compositeness scale $\Lambda$ using the dijet angular distributions.

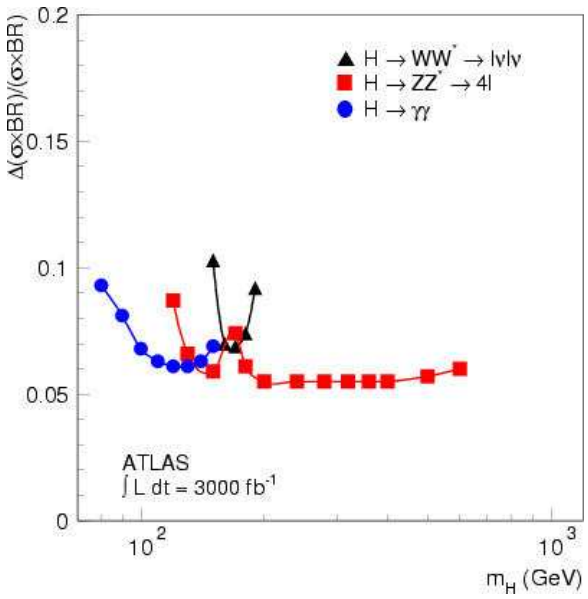


Figure 3: Expected precision on the measurement of Higgs boson production rates for at 14 TeV and very high luminosity.

ments of couplings will be limited by the available statistics and could benefit from an upgrade. The following final states are expected to be observable depending upon the mass: $\gamma\gamma$, $\tau\tau$, $ZZ \to \ell\ell\ell\ell$, $WW \to \ell\nu\ell\nu$ and $b\overline{b}$. The relevant production processes are $qq \to qqH$ (the vector boson fusion process) which depends upon the $HWW$ and $HZZ$ couplings, $gg \to H$ via a loop involving, in particular, top quarks, $q\overline{q} \to HW$, and $gg \to t\bar{t}H$ which is sensitive to the $ttH$ coupling. Studies of the expected precision for the benchmark LHC [3] have been extended for the upgrade scenarios. The expected precision on the production rates is shown in Figures 3 and 4. In these plots it is assumed that there is an error of 5% on the measurement of the absolute luminosity. In some cases this becomes the limiting factor. Figure 3 shows the measurements for final states containing gauge bosons produced by the gluon-gluon fusion process. Figure 4 shows that for the other processes. In the mass range below 200 GeV which is favored by fits to electroweak data [4], there are a large number of possible measurements. The factor of ten increase in luminosity over the standard LHC scenario improves the precision by approximately a factor of two and brings many of these measurements to the point where they are limited by the uncertainty on the measurement of the luminosity and other systematic effects. In particular, we have assumed that the measurement of $tau\tau$ final state does not improve at very high luminosity due to the difficulties of reconstructing these states. Also the $WW$ final state is compromised by the background as it has no mass peak and the uncertainty in the shape of this background contributes to the uncertainty.

Once these cross-section measurements are made, they can be used to extract information on the couplings of the Higgs boson. In the case where measurements of different final states are made from the *same* Higgs production mechanism, a direct measurement of the ratios of Higgs couplings is possible. Figure 5 shows the expected precision on the ratio of the Higgs partial widths to the $WW$ and $ZZ$ final states. For masses greater than approximately 160 GeV measurements of $H \to ZZ \to 4\ell$ and $H \to WW \to \ell\nu\ell\nu$ rates from the same production process enables a direct (model independent) measurement to be made. At smaller masses the process $H \to WW \to \ell\nu\ell\nu$ has too low a rate but an indirect measurement can be obtained by combining the measured rates

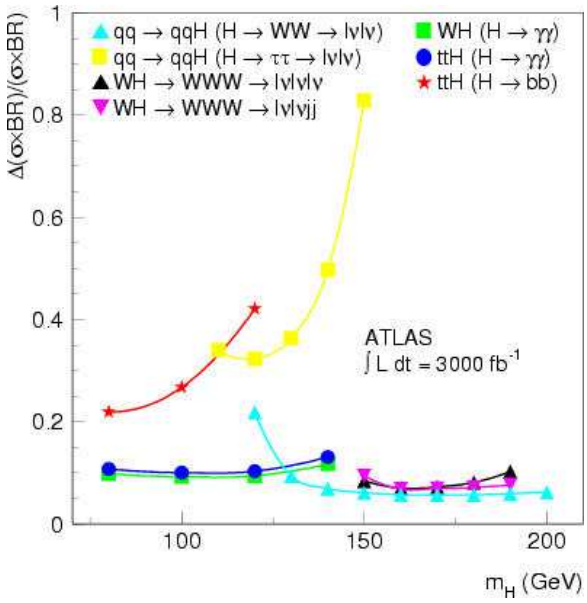


Figure 4: Expected precision on the measurements of the production rates of the Higgs boson in various channels at 14 TeV and very high luminosity.

for $H \to ZZ \to 4\ell$ and $H \to \gamma\gamma$ and making a theoretical assumption. The coupling $H \to \gamma\gamma$ is dominated by a loop graph with an intermediate $W$ and hence the rate $H \to \gamma\gamma$ can be related to the $HWW$ coupling.

Measurements of the fermion couplings shown in Figure 6 are more difficult. Events with $H \to \tau\tau$ and $H \to WW \to \ell\nu\ell\nu$ and tagged forward jets arise from the same production process ($qq \to qqH$) and hence can be combined to directly measure $\Gamma_W/\Gamma_\tau$ as shown in Figure 6. The coupling $Ht\bar{t}$ can be probed by comparing the $WH \to \ell\nu\gamma\gamma$ and $H \to \gamma\gamma$ rates. The latter production rate is determined by the coupling of Higgs to gluon pairs and the dominant contribution to this coupling is from a top quark loop which probes the $Ht\bar{t}$ coupling strength. An indirect measurement of the ratio of couplings $HWW$ and $Ht\bar{t}$ can therefore be made and is shown on Figure 6 Similarly the final states $t\bar{t}H(\to \gamma\gamma)$ and $t\bar{t}H(\to b\bar{b})$ can be combined to give the ratio of widths to $b\bar{b}$ and $WW$ shown as an indirect measurement in Figure 6. Again the increased luminosity improves the precision of the measurements by approximately a factor of two.

If the energy of the LHC were raised to 28 TeV, then for a Higgs boson of mass $\sim 150$ GeV ($\sim 1$ TeV), the Higgs production cross-section would rise by a factor of 2 (8). Therefore, in the case of Higgs masses at the lower end of the search range, the luminosity upgrade is much more powerful. However, it is important to emphasize that the full detector functionality and performance must be maintained at the upgraded luminosity if this advantage is to be exploited.

In the case of SUSY Higgs bosons there are regions of the MSSM parameter space where only the lightest Higgs state ($h$) will have been seen at LHC. In this case the sensitivity to the heavier Higgs states via for the decays $A \to \tau\tau$ and $A \to \mu\mu$ will be increased at an upgraded LHC. In the case of $m_A = 500$ GeV the energy upgrade increases the H/A cross-section by approximately a factor of five thereby increasing the discovery potential for heavy Higgs bosons.

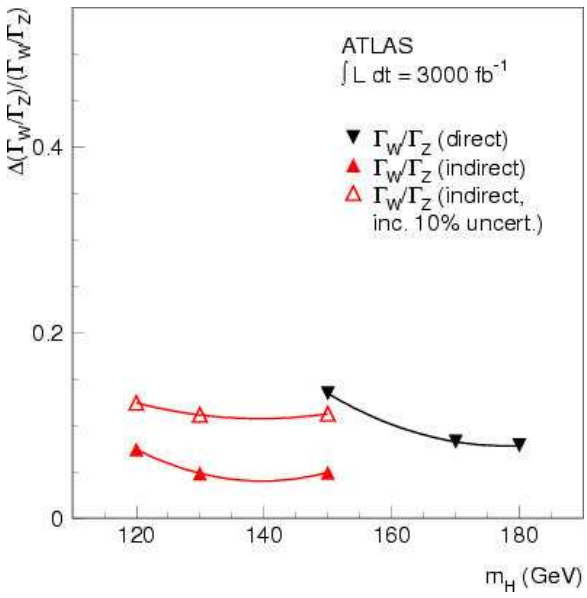


Figure 5: Expected fractional error on the measured ratio of Higgs partial widths to $WW$ and $ZZ$ as a function of the Higgs mass. The results labeled direct are obtained with no additional theoretical assumptions. Those labeled indirect have additional assumptions (see text). Also shown is the effect of a 10% uncertainty in the theoretical assumptions.

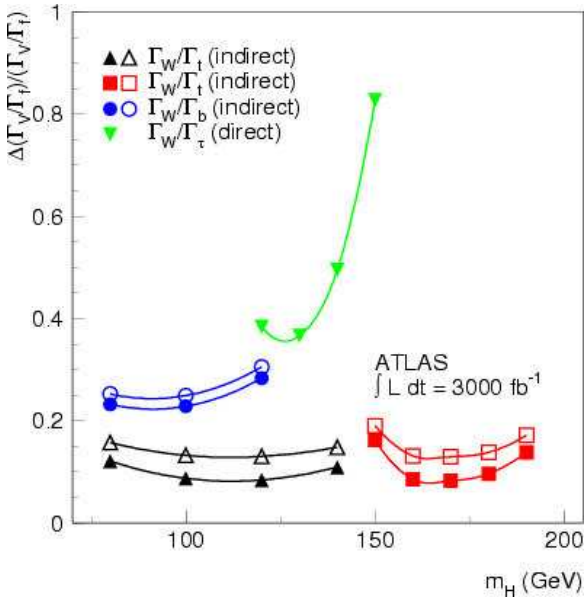


Figure 6: Expected fractional error on the measured ratio of Higgs partial widths to several final states as a function of the Higgs mass. The widths shown are $\tau\tau$, $WW$ and $b\overline{b}$. The results labeled direct are obtained with no additional theoretical assumptions. The top quark coupling strength $\Gamma_t$, is inferred from other measurements (see text). The open symbols contain an additional 10% theoretical uncertainty.

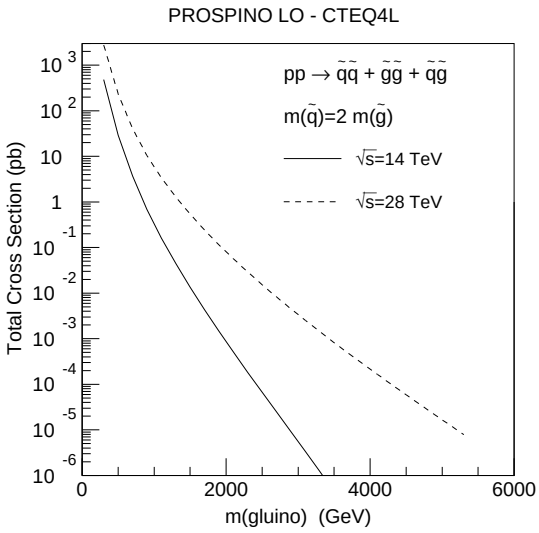


Figure 7: The total SUSY production cross section as a function of the gluino mass for the case where $m_{\tilde{q}} = 2.0 m_{\tilde{g}}$.

# 4 Supersymmetry studies

Perhaps the strongest argument for weak scale SUSY is that it allows light Higgs bosons without unnatural fine tuning in the presence of much heavier scales such as the Planck mass. While the concept of fine tuning is not precise, there is a general consensus that this requires SUSY particles to be lighter than about 1 TeV; see, *e.g.*, [5]. Masses in this range are also consistent with grand unification, cold dark matter, an observable SUSY contribution to $g_\mu - 2$ [6, 7], and a variety of other constraints [8, 9, 10, 11, 12].

If $R$ parity is conserved, all SUSY particles decay to the lightest SUSY particle (LSP) $\tilde{\chi}_1^0$, which escapes the detector. Thus, the production of gluinos or squarks provides signatures with multiple jets, possibly leptons, and missing transverse energy $\not\!\!E_T$. In typical SUSY breaking scenarios such as minimal SUGRA [13], the LHC should discover evidence for gluinos or squarks up to 1 TeV in the $\not\!\!E_T$ + jets channel with an integrated luminosity of $1\,\mathrm{fb}^{-1}$ or less; the ultimate discovery reach for $300\,\mathrm{fb}^{-1}$ extends beyond 2.5 TeV.

The increase in mass reach for squarks and gluinos at higher LHC energy is evaluated approximately by comparing the squark and gluino production cross-sections at 14 and 28 TeV. The primary Standard Model backgrounds, $t\bar{t}$ production and W/Z+jets increase due to the larger center of mass energy. However, this effect will be more than compensated by the harder cuts on the transverse energy flow and missing $E_T$ in the events which can be applied compared to the analysis performed for a 14 TeV collider. The cross-section was evaluated at leading order using the program PROSPINO [14] with CTEQ4L [15] structure functions. Three scenarios were considered: $m_{\tilde{q}} = 2m_{\tilde{g}}$, $m_{\tilde{g}} = 2m_{\tilde{q}}$, $m_{\tilde{g}} \sim m_{\tilde{q}}$. The total cross section for the production of squarks and gluinos is given in the Figures 7, 8 and 9 as a function of the mass of the lighter sparticle be it squark or gluino in these scenarios.

An approximation of the reach at 28 TeV is obtained by taking the masses for which the signal cross-section is equal to the one for the maximum reachable masses at 14 TeV [1], *i.e.* around $10^{-2}$ pb for 100 $\mathrm{fb}^{-1}$. The approximate SUSY mass reach for an integrated luminosity of 100 $\mathrm{fb}^{-1}$ at

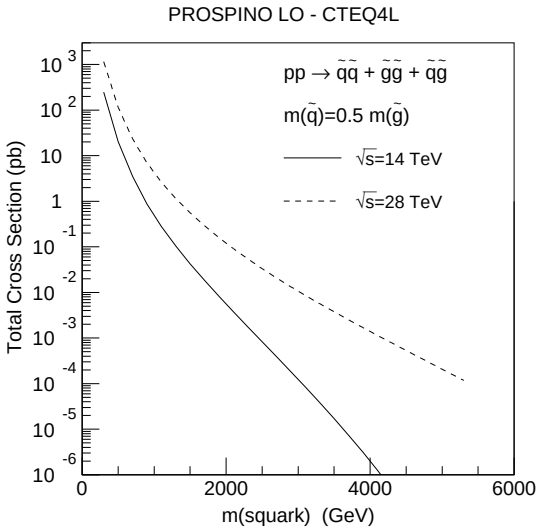


Figure 8: The total SUSY production cross section as a function of the squark mass for the case where $m_{\tilde{q}} = 0.5 m_{\tilde{g}}$.

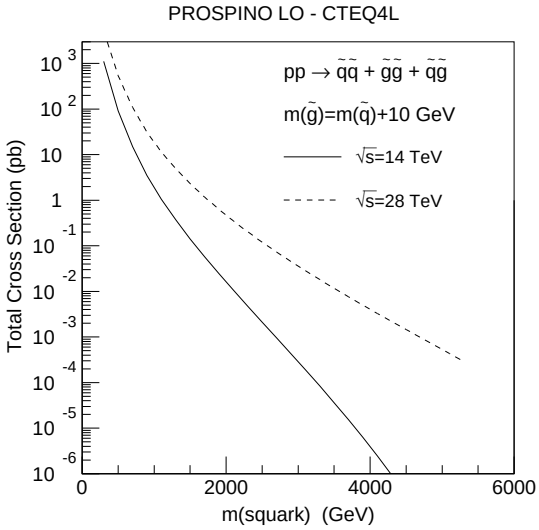


Figure 9: The total SUSY production cross section as a function of the squark mass for the case where $m_{\tilde{g}} = m_{\tilde{q}} + 10$ GeV.

| scenario | 14 TeV 100 fb$^{-1}$ | 14 TeV 1000 fb$^{-1}$ | 28 TeV 100 fb$^{-1}$ | 28 TeV 1000 fb$^{-1}$ |
|---|---|---|---|---|
| $m_{\tilde{q}} \sim m_{\tilde{g}}$ | 2.1 | 2.7 | 3.9 | 4.4 |
| $m_{\tilde{q}} = 2m_{\tilde{g}}$ | 2.0 | 2.3 | 2.7 | 4.2 |
| $m_{\tilde{g}} \sim 2m_{\tilde{q}}$ | 1.9 | 2.2 | 2.9 | 4.1 |

Table 3: Comparison of the reach in squark masses in TeV in the different scenarios. In each case a nominal one year of running is assumed.

28 TeV is thus: 3.9 TeV for $m_{\tilde{q}} \sim m_{\tilde{g}}$, 2.7 TeV for $m_{\tilde{q}} = 2m_{\tilde{g}}$, and 2.9 TeV for $m_{\tilde{g}} \sim 2m_{\tilde{q}}$, which corresponds to an approximate doubling of the accessible mass range. An increase in the luminosity is somewhat less powerful as can be seen from Table 3, but it still provides a mass reach 20% higher than the standard LHC scenario reaching 2.7 TeV for the case $m_{\tilde{q}} \sim m_{\tilde{g}}$.

Given the naturalness arguments made above it is almost guaranteed that SUSY will be discovered at the baseline LHC if it is relevant to the problem of electroweak symmetry breaking. Thus, the role of an LHC upgrade in energy, luminosity, or both would be to complete the spectrum and make additional precise measurements. What measurements might be of interest many years after the first discovery of SUSY is of course model dependent and difficult to predict. It seems likely, however, that these measurements will require the full capability of ATLAS including good identification and measurements of $e$'s, $\mu$'s, $\tau$'s, jets, $b$-jets, and $\not\!\!E_T$.

While gauginos are likely to be lighter than 1 TeV, sfermions might be heavier. In the "inverted hierarchy" scenario [16], all scalars are heavy at the GUT scale. With appropriate GUT boundary conditions the renormalization group equations drive the third generation sfermions below 1 TeV but leave the rest heavy, perhaps several TeV. In the "focus point" scenario [17], even the stops ($\tilde{t}_{1,2}$) can have multi-TeV masses. In scenarios like these, gluinos and their decay products would still be discovered quickly at the LHC, but some or all of the squarks and sleptons would be inaccessible. A search for very massive squarks might impose fewer constraints on the detector performance than precision measurements at very high luminosity, but no simulation has been done. Models with very massive sfermions often lead to many competing gluino decay modes, each with a small branching ratio. Precision measurements of gluino processes at the LHC could be rate limited and might also benefit by an upgrade.

SUGRA Point 2 from [1] was chosen as an example of the possible gains for SUSY studies from an energy or luminosity upgrade of the LHC. This point has $m_0 = m_{1/2} = 400\,\text{GeV}$, $A_0 = 0$, $\tan\beta = 10$, and $\text{sgn}\,\mu = +$, giving gluino and squark masses of about 1 TeV. While discovery of a signal in the $\not\!\!E_T$ + jets channel is straightforward, the precision measurements discussed in Ref. [1] were relatively difficult. The channel $\tilde{\chi}_2^0 \to \tilde{\chi}_1^0 Z$, $Z \to \ell^+\ell^-$ was not used because of the small rate as can be seen in Fig. 20-25 of Ref [1] which shows an inclusive sample of 70 events for an integrated luminosity of 30 fb$^{-1}$. A luminosity upgrade would clearly result in an event sample large enough to do a detailed study provided the detector performance can be maintained. At 28 TeV the total SUSY production cross section is increased to 37 pb from 3.2 pb at 14 TeV showing that in this example the luminosity and energy upgrades are almost the same in their effect on the production rates. In an attempt to exploit the larger event rates, events were selected with cuts similar to those used in [1] using ISAJET 7.51 [19]:

- At least 4 jets with $p_T > 100, 50, 50, 50\,\text{GeV}$;
- $M_{\text{eff}} > 1000\,\text{GeV}$;

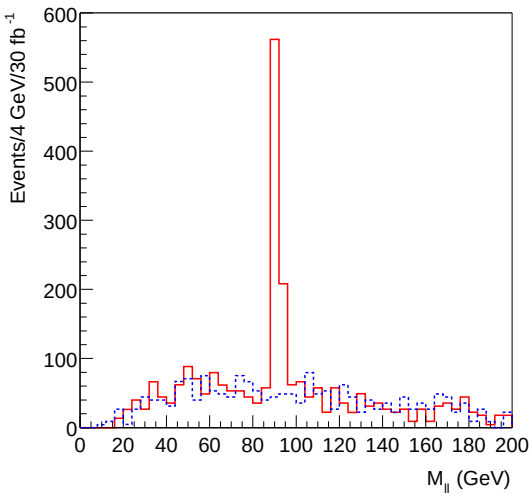


Figure 10: $\ell^+\ell^-$ mass distribution at SUGRA Point 2 at 28 TeV.

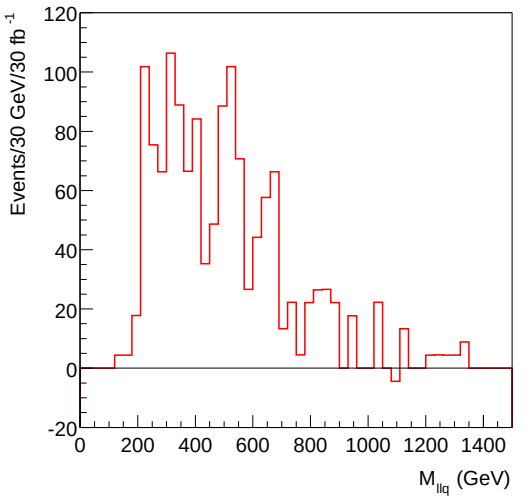


Figure 11: $\ell^+\ell^- j$ mass distribution formed from $\ell^+\ell^-$ in the $Z$ mass peak plus one of the two hardest jets at SUGRA Point 2 at 28 TeV.

- $\not{E}_T > 0.2 M_{\rm eff}$;
- $S_T > 0.2$.

where

$$M_{\rm eff} = p_{T,1} + p_{T,2} + p_{T,3} + p_{T,4} + \not{E}_T \, .$$

and $S_T >$ is the transverse sphericity. Standard Model backgrounds were not generated, but they should be small after these cuts are made, as shown in [1]. Leptons ($e$,$\mu$) were required to have $p_T > 10$ GeV and to be isolated with $E_T < 10$ GeV in a cone of $R = 0.4$ around the lepton direction. The dilepton mass distribution with these cuts is shown in Fig. 10. The $Z \to \ell^+\ell^-$ peak now has

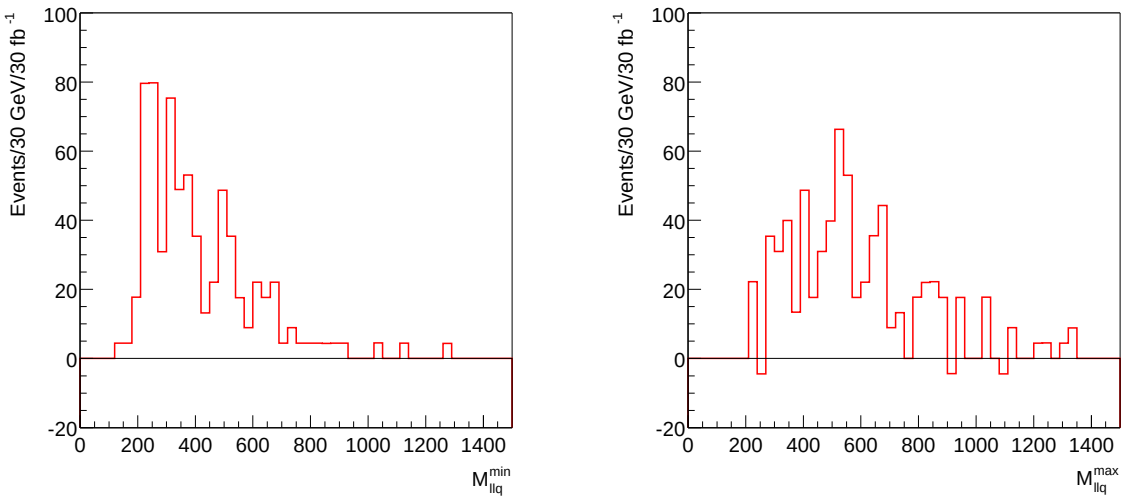


Figure 12: Minimum (left) and maximum (right) masses selected as in Fig. 11.

more than 500 events for an integrated luminosity of 30 fb$^{-1}$. Thus either the energy or luminosity upgrade produces an event sample large enough to perform further analyses.

For example, the main source of $\tilde{\chi}_2^0$ at Point 2 is $\tilde{q}_L \to \tilde{\chi}_2^0 q$. The two hardest jets in SUSY events are expected to come from $\tilde{q}$ decays. The $\ell^+\ell^- q$ mass distribution formed by combining the two leptons in the $Z$ mass peak with each of the two hardest jets is shown in Fig. 11. The smaller of these masses should be less than the kinematic upper limit for $\tilde{q}_L \to \tilde{\chi}_2^0 q \to \tilde{\chi}_1^0 Z q$, while the larger should be greater than the kinematic lower limit. These distributions are shown in Fig. 12. In either upgrade scenario the statistics are sufficient to make measurements that significantly constrain the squark and $\tilde{\chi}_2^0$ masses in a manner that would not be possible with the baseline LHC.

## 5 Jet tagging/vetoing at higher luminosity

The presence of jets at large rapidity can be used to enhance the signal-to-background ratio in certain processes such as those involving $WW$ fusion where the $W$'s are emitted from quarks (see, for example, 19.2.10.1 of Ref [1]). Similarly the absence of jets at central rapidity can be used to enhance processes involving the production of particles with only electroweak charges relative to the production of strongly coupled particles (see, for example, section 19.2.10.2 of Ref [1]). As the luminosity increases both of these selections are expected to become less useful as the pile-up of additional events can cause jets to appear in these regions as well as degrading the measurements of the jets used for tagging/vetoing.

An estimate of the effects was obtained using a full simulation study of pileup in the ATLAS detector. Pileup from the appropriate number of minimum bias events in up to 25 beam crossings before and 3 beam crossings after $t = 0$ was generated, taking into account the response of the different calorimeters. Jets were then found using a jet finder with cone size $\Delta R = 0.4$ or $\Delta R = 0.2$, and assigned to ranges of rapidity

- Forward: $\eta > 2.0$

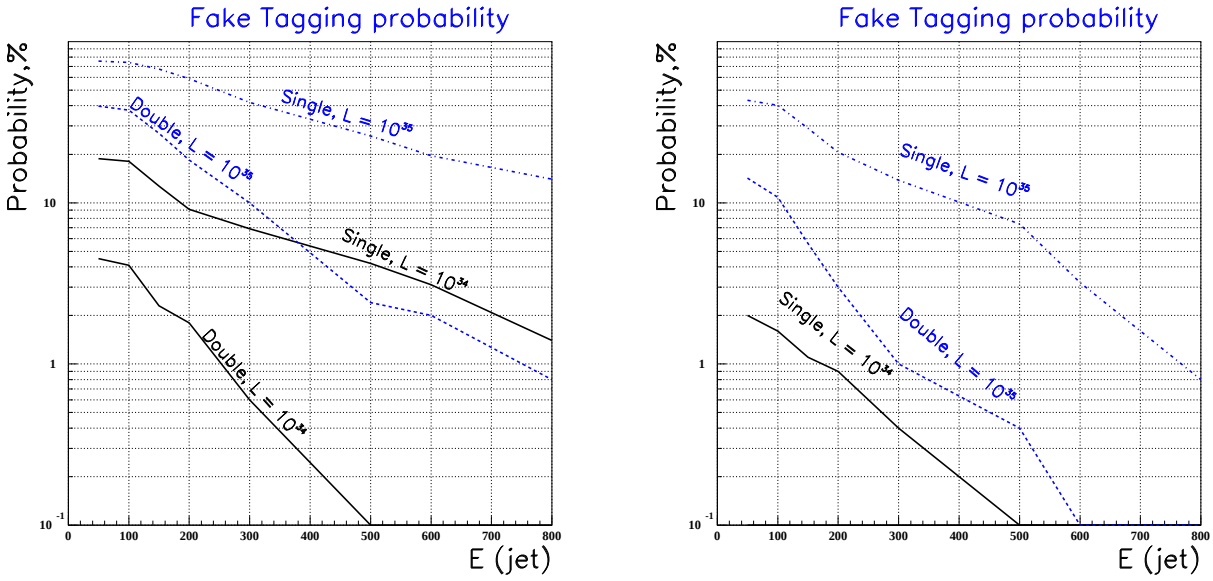


Figure 13: Estimate of the probability of single and double forward jet tagging from pile-up, for nominal and very high luminosities, at 14 TeV, as a function of the jet energy, and for $\Delta R = 0.4$ (left) and $\Delta R = 0.2$ (right).

- Backward: $\eta < -2.0$
- Central: $|\eta| < 2.$

A single tag is defined as an event with either a forward or backward jet; a double tag has both. The probability of an event consisting only of minimum bias interactions having either a single or double jet tag is shown in Figure 13 as a function of the jet energy. The probability of an event having an additional central jet is shown in Figure 14 as a function of $p_T$. The values plotted in these figures are approximate, and depend sensitively on jet energy calibration and reconstruction conditions. At a luminosity of $10^{35}$ cm$^{-2}$ sec$^{-1}$ the pile up of minimum bias events renders forward jet tagging and central jet vetoing difficult. The performance that is assumed here may be too pessimistic as it may be possible to reduce the pile-up noise in the LAr calorimeter by using optimal filtering techniques at the upgraded luminosity [21] and optimizing the jet algorithm. At an energy of 28 TeV, the average number of minimum bias events increases by about 15% and the energies and multiplicities of particles in these events is higher. In this case, as a rough approximation, it will be assumed that the rates of fake forward jet tags and of extra central jets are twice as big as at nominal luminosity.

This tagging result has implications for strong $WW$ scattering signals as is now discussed.

## 6 Strongly coupled Vector Boson system

If there is no light Higgs boson, then general arguments [22] imply that scattering of electroweak gauge bosons at high energy will show structure beyond that expected in the Standard Model. In order to explore such signals it is necessary to measure final states of pairs of gauge bosons with large invariant mass.

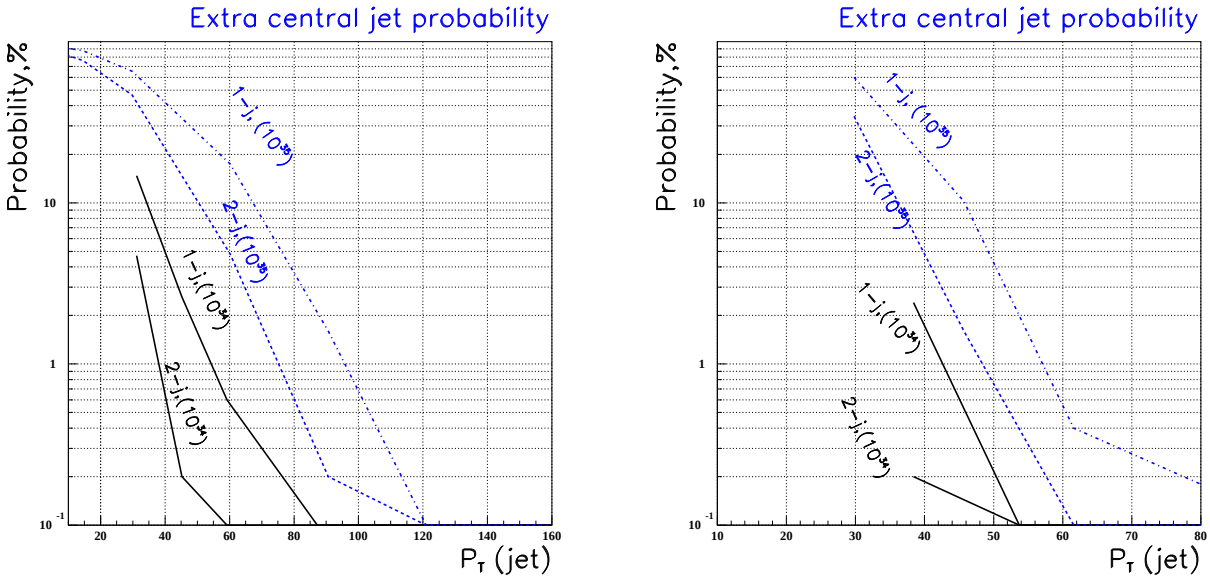


Figure 14: Estimate of the probability of one or two extra central jets from pile-up, for nominal and very high luminosities, at 14 TeV, as a function of the jet $p_T$ threshold, and for $\Delta R = 0.4$ (left) and $\Delta R = 0.2$ (right).

| Process | $\sigma$ (pb) |
|---|---|
| $qq \to qqWZ$ | 1.45 |
| $Zb\bar{b}$ | 141 |
| $Zt\bar{t}$ | 2.23 |
| $qq \to WZ$ | 3.00 |
| $qq \to ZZ$ | 0.81 |

Table 4: Cross sections for backgrounds to the $W_L Z_L \to W_L Z_L$ process

### 6.1 $W_L Z_L \to W_L Z_L$

Estimates of the production of a $\rho$-like vector resonance of $W_L Z_L$ can be obtained from the Chiral Lagrangian model, with the inverse amplitude method of unitarization [23]. The cross section depends, in next to leading order, on a linear combination $a_4 - 2a_5$ of two quadrilinear coupling parameters. The model was implemented in PYTHIA. Only the channel $W_L Z_L \to W_L Z_L \to \ell\nu\ell^+\ell^-$ is here considered, although the resonance can be produced in the $q\overline{q}$ fusion channel at higher rate. Forward jet tagging is here an essential ingredient to reduce the background.

The irreducible Standard Model background $qq \to qqWZ$, with transverse gauge bosons in the final state was generated with COMPHEP [24] with cuts $p_T(q, W, Z) > 15$ GeV, and $m_{WZ} > 500$ GeV, with CTEQ5L structure functions and $Q = M_Z$. The process includes electroweak and QCD diagrams, as well as the quadrilinear gauge boson couplings. The Higgs mass was set at the low value of 100 GeV, and the signal is then defined, as in [25], as the enhancement of the SM prediction over the 100 GeV Higgs. Other background considered were $Zb\bar{b}$ and $Zt\bar{t}$, also generated with COMPHEP, with cuts $p_T(b, t) > 15$ GeV and $p_T(Z) > 50$ GeV, and SM production of $WZ$, $ZZ$, generated with PYTHIA. Table 4 gives the cross sections for the different backgrounds.

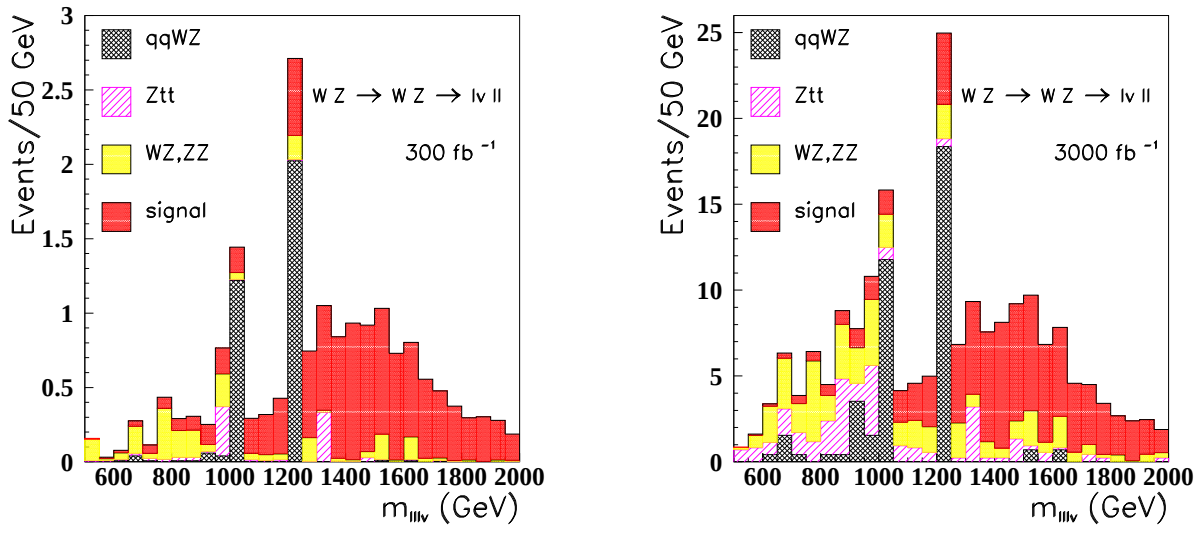


Figure 15: Expected signal and background for a 1.5 TeV WZ resonance in the leptonic decay channel with 300 fb$^{-1}$ (left) and 3000 fb$^{-1}$ (right).

The selection criteria required leptonic cuts:

$$p_T(\ell_1) > 150\text{GeV}, \quad p_T(\ell_2) > 100\text{GeV}, \quad p_T(\ell_3) > 50\text{GeV}$$
$$|m(\ell_1\ell_2) - m(Z)| < 10\text{GeV}$$
$$\not{E}_T > 75\text{GeV}$$

and forward jet tagging, i.e. the presence of one forward and one backward jets ($|\eta| > 2$) with energy greater than 300 (400) GeV at nominal (very high) luminosities, as well as a veto if a jet with transverse momentum greater than 50 (70) GeV at nominal (very high) luminosity was present in the central region ($|\eta| < 2$).

Fig. 15 shows the expected signal for a 1.5 TeV resonance, corresponding to a choice of Chiral Lagrangian parameters $a_4 - 2a_5 = 0.006$, at nominal LHC and at an upgraded LHC with tenfold luminosity, taking into account the effects of pileup according to Figs. 13 and 14, with $\Delta R = 0.4$. The resonance is at the limit of observation at LHC, with 6.6 events expected over a background of about 2.2 around the region of the peak, but at very high luminosity the signal has an approximate significance $S/\sqrt{B} = 48/\sqrt{16} = 12$.

### 6.2 $Z_LZ_L$ scalar resonance

Production of a scalar $Z_LZ_L$ resonance decaying by the golden channel $ZZ \to 4\ell$ is a rare process, well suited to an upgraded LHC. As for the $WZ$ resonance above, the Chiral Lagrangian model, with regularization by the inverse amplitude method [23] was used. The cross section depends on a linear combination, $7a_4+11a_5$, of the same parameters as those of the vector resonance and therefore observation of the scalar resonance will help resolve $a_4$ and $a_5$ unambiguously. The $ZZ$ production signal occurs through the scattering processes $W_L^+W_L^- \to Z_LZ_L$ and $Z_LZ_L \to Z_LZ_L$. Standard Model background, leading to $qqZZ$ in the final state have been generated with COMPHEP, with cuts $p_T(q, Z) > 15$ GeV, $m_{ZZ} > 500$ GeV, $m_{qq} > 200$ GeV, with CTEQ5L as parton distribution function and $Q = m_Z$. The process was implemented in PYTHIA as an external process.

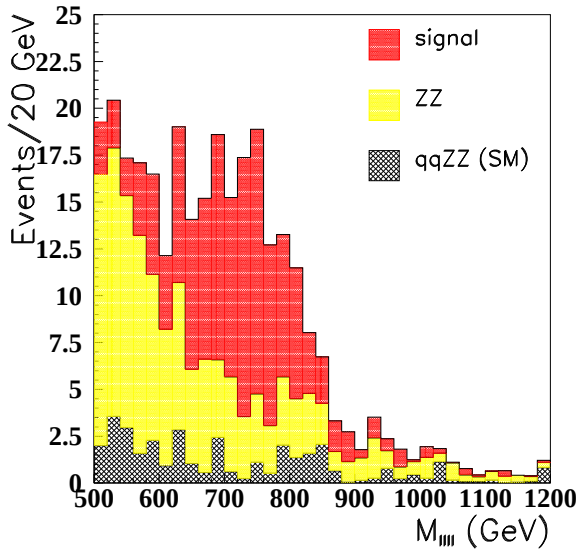


Figure 16: Reconstructed ZZ mass from the leptonic decay of a scalar resonance of 800 GeV.

The Higgs mass was set at 100 GeV so that the contribution from longitudinal vector boson scattering was negligible in this background. With these conditions, the SM cross section is 69.4 fb. Other backgrounds considered were $qq \to ZZ$, with cuts $m_{ZZ} > 500$ GeV, and cross section 8.66 fb. The background $gg \to ZZ$ was not included, but is expected to contribute about one third of the $q\bar{q}$ fusion process [23].

The analysis requires the presence of four isolated leptons having a transverse momentum greater than 30 GeV, and leading to the reconstruction of two $Z$'s. The identification efficiency of electrons was taken to be 80% and those of muons 90%. Forward jet tagging was applied by requiring the presence of one forward and one backward jet ($|\eta| > 2$) with energies greater than 400 GeV. No central jet veto was imposed, as the main backgrounds do not justify it. Fake tagging by pileup was taken into account, according to the results in Fig. 13, with $\Delta R = 0.4$. With an integrated luminosity of 3000 fb, for a 14 TeV collider, the expected signal and background for a resonance at 750 GeV, corresponding to $7a_4 + 11a_5 = 0.063$ is shown in Fig. 16. Such a process would not be observable at the nominal LHC.

### 6.3 $W_L^+W_L^+$

Non-resonant production of vector boson pair at high mass presents a challenge at LHC because the level of background needs to be very well understood.

Production of $W^+W^+$ pairs has no contribution from $q\overline{q}$ fusion. Two models have been considered:

- A Higgs boson of mass 1 TeV (as a reference point).
- WW production with K-matrix unitarization.

Backgrounds arise from gauge boson pairs produced by electroweak and gluon exchange diagrams [1]. Here the promising $\ell^+\ell^+\nu\nu$ final state arising from $W^+W^+$ production is studied. The analysis cuts are essentially the same as in [1], consisting of leptonic cuts

| | 300 fb$^{-1}$ 14 TeV | 3000 fb$^{-1}$ 14 TeV | 300 fb$^{-1}$ 28 TeV | 3000 fb$^{-1}$ 28 TeV |
|---|---|---|---|---|
| Forward tag $E$ | 400 | 600 | 600 | 800 |
| Forward tag $p_T$ | 90 | 90 | 150 | 150 |
| Central veto | 40 | 60 | 50 | 100 |

Table 5: Energies of the two forward jets required for tagging and the transverse momentum of the central jets used for vetoing in GeV for the various energies and luminosities in the study of $W^+W^+$ final states. The forward jets were also required to have a transverse momentum less than shown.

| Model | 300 fb$^{-1}$ 14 TeV | 3000 fb$^{-1}$ 14 TeV | 300 fb$^{-1}$ 28 TeV | 3000 fb$^{-1}$ 28 TeV |
|---|---|---|---|---|
| Background | 7.9 | 44 | 20 | 180 |
| K-matrix Unitarization | 14 | 87 | 57 | 490 |
| Significance | 3.0 | 7.6 | 6.5 | 18.9 |
| Higgs, 1 TeV | 7.2 | 42 | 18 | 147 |
| Significance | 1.8 | 4.5 | 2.9 | 8.1 |

Table 6: Numbers of reconstructed events above an invariant mass of 600 GeV (for 14 TeV) and 800 GeV (28 TeV) for models of a strongly coupled Higgs sector and for the background. The significance was computed as $S/\sqrt{S+B}$.

- two leptons ($e$ or $\mu$) reconstructed in the central region, $|\eta| < 1.75$, of positive charge and having $p_T > 40$ GeV
- The difference in azimuthal angle of the two leptons, $cos(\Delta\phi(\ell\ell)) < -0.5$ $(-0.8)$ for 14 (28) TeV collisions
- $\Delta p_t(ll) = |\vec{p}_T(\ell_1) - \vec{p}_T(\ell_2)| > 100$ GeV for the 28 GeV case.
- missing transverse energy $E_T^{miss} > 40$ (50) GeV for 14 (28) TeV collisions

The jet tagging and vetoing cuts were varied as a function of the energy and luminosity as shown in Table 5. Two forward tagging jets with energies above the amount shown in the table were required and events were vetoed if there was a central jet with transverse momentum greater than the indicated amount. Table 6 shows the number of events expected and their significances for a typical set of cuts, for 300 fb$^{-1}$ at nominal luminosity and 3000 fb$^{-1}$ at very high luminosity at 14 and 28 TeV. In the case of ultra high luminosity electron identification efficiency is assumed to be 80%. It may be possible to reduce the effects of pile up by improving filtering and optimising the jet tagging.

The increase in energy to 28 TeV would enhance considerably the sensitivity to high mass vector boson pair production, even in a non-resonant scenario. The study of the signal could be pushed from a limit of about 1 TeV in the invariant mass of the $WW$ system to around 1.5 TeV. Fig. 17 shows the signal and background distributions as a function of the invariant mass formed from the two leptons and the missing transverse momentum (*c.f.* Figure 19-110 of [1]). In spite of the apparent increase in statistical significance, the systematic errors are likely to be very high

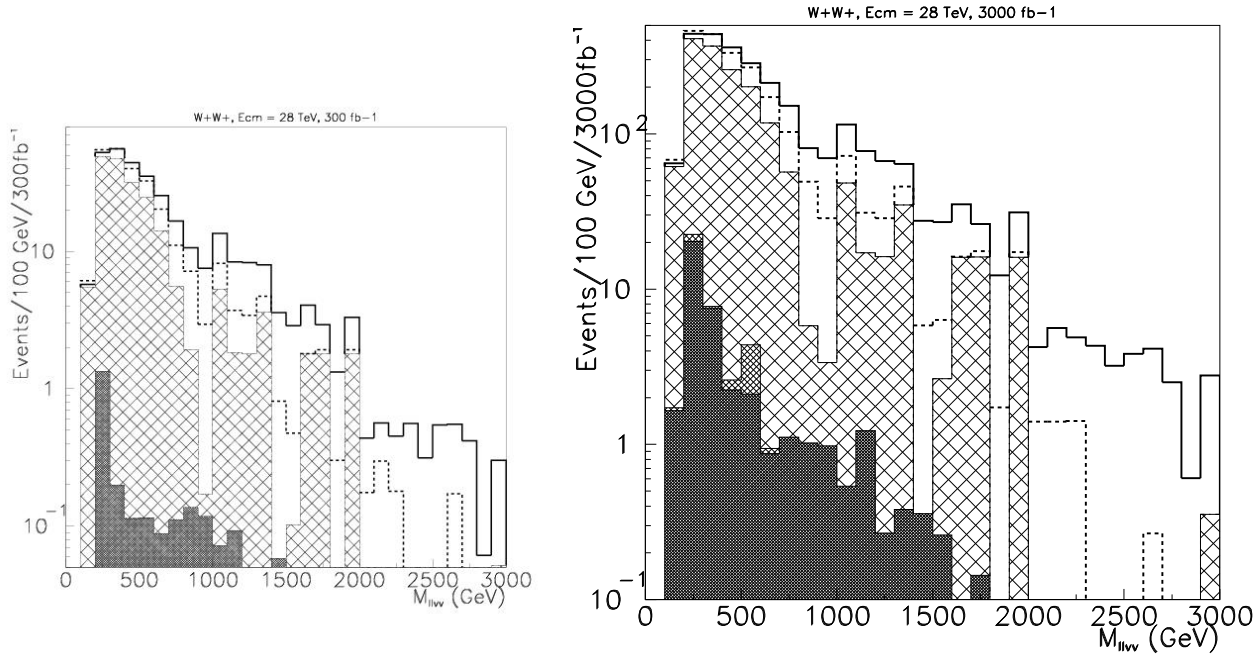


Figure 17: Signals from strong WW scattering at 28 TeV and 300 fb$^{-1}$ (left) and 3000 fb$^{-1}$ (right) of integrated luminosity. Event rates are shown as a function of the invariant mass of the $\ell\ell\not{E}_T$ system. The backgrounds are shown as histograms, from inside to outside (or darker to lighter): WZ continuum: W pairs (transverse) from gluon exchange diagrams: W pairs (transverse) from electroweak ($\gamma$ and Z exchange) diagrams. The possible signals are: continuous line, K-matrix unitarization: dashed line: Higgs, 1 TeV.

since the shapes of the backgrounds and signal are similar. The extraction of signals should be done with many different choices of cuts so as to verify the dependence on the cuts and constrain the systematics. This analysis can only be an estimate of the reach. At high luminosities a good understanding of jet reconstruction and backgrounds will be needed.

# 7 Extra dimensions

One of the possible signals expected from large extra dimensions is the production of jets or photons in association with missing transverse energy. The former channel is more sensitive so will be considered here. The background is dominated by the final state $Z(\rightarrow \nu\nu) + jets$ [26].

In order to assess the impact of the possible upgrades a study using ATLFAST [20] was made. The signal is characterized by two parameters, the number of extra dimensions $\delta$ and the scale $M_D$ characterizing the scale of gravity. Table 7 shows the maximum value of $M_D$ that can be detected for a given value of $\delta$ in the four scenarios.

It can be seen from the table that doubling the LHC energy to 28 TeV approximately doubles

| $\delta$ | 14 TeV 100 fb$^{-1}$ | 14 TeV 1000 fb$^{-1}$ | 28 TeV 100 fb$^{-1}$ | 28 TeV 1000 fb$^{-1}$ |
|---|---|---|---|---|
| 2 | 9 | 12 | 15 | 19 |
| 3 | 6.8 | 8.3 | 11.5 | 14 |
| 4 | 5.8 | 6.9 | 10 | 12 |

Table 7: 5 $\sigma$ discovery reach on $M_D$, in TeV, as a function of the number of extra dimensions ($\delta$) for various values of energy and integrated luminosity.

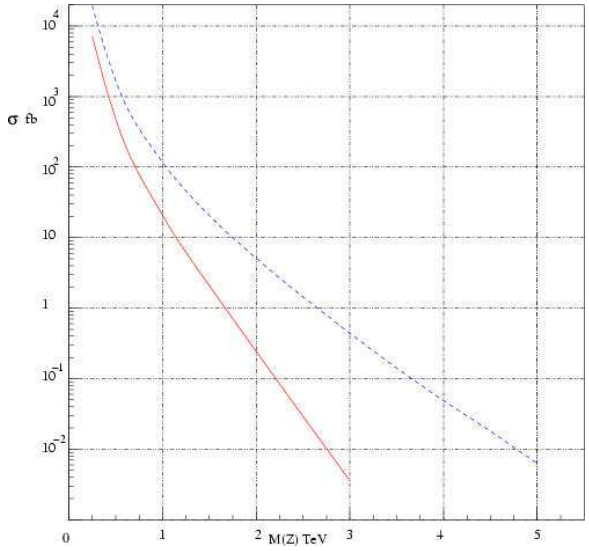


Figure 18: Production rate for $Z' \to \mu^+\mu^-$ at 14 and 28 TeV as a function of the $Z'$ mass.

the reach in $M_D$ for any value of $\delta$. An increase in the integrated luminosity by a factor of 10 raises the reach by approximately 30%. If a signal is observed at 14 TeV, the energy increase is such that model dependent signals can be expected to be observed at 28 TeV. Such observations would therefore provide valuable insight into the dynamics of the underlying theory. Detector performance is not expected to be critical as events with jets and missing energy in the TeV range are relevant for this search.

# 8 Searches for New Gauge Bosons

As an example of the impact of the possible upgrades, Figure 18 shows the production rate for $\mu^+\mu^-$ final states arising from the decay of a $Z'$ gauge boson with the same couplings to quarks and leptons as the Standard Model $Z$ as a function of the mass of the $Z'$. The final state $e^+e^-$ is not considered, because it is more difficult to exploit at the highest luminosity particularly if the tracker is not upgraded. The calorimeter can still be used to detect this channel but the signs of the electrons cannot be determined and measurements of asymmetries cannot be undertaken. If this channel were included and had the same acceptance as the muon channel, the mass reach would increase by approximately 20%.

The discovery limit for $Z' \to \mu^+\mu^-$ is given in Table 8 from which it can be seen that the combination of energy and luminosity upgrade doubles the mass reach.

| 14 TeV 100 fb$^{-1}$ | 14 TeV 1000 fb$^{-1}$ | 28 TeV 100 fb$^{-1}$ | 28 TeV 1000 fb$^{-1}$ |
|---|---|---|---|
| 4.5 | 5.4 | 7.0 | 9.5 |

Table 8: $5\sigma$ discovery reach in $Z'$ mass in TeV in the $\mu^+\mu^-$ final state, for a $Z'$ with the same couplings to quarks and leptons as the Standard Model $Z$.

The decay $Z' \to WW \to \ell\nu jj$ (see Section 21.6.1.4 of [1]) has also been studied. This channel is not competitive for discovery but can provide important information on the couplings of the $Z'$. This study uses the final state where the lepton is a muon, as electron detection will be more difficult at higher luminosity. The mass reachable in this final state is shown in Table 9.

| | 14 TeV 300 fb$^{-1}$ | 14 TeV 3000 fb$^{-1}$ | 28 TeV 300 fb$^{-1}$ | 28 TeV 3000 fb$^{-1}$ |
|---|---|---|---|---|
| Mass (TeV) | 1.9 | 2.5 | 2.4 | 3.3 |

Table 9: $5\sigma$ discovery reach in TeV for a $Z'$ observed in the $WW \to \mu\nu jj$ final state.

The ability to measure muons and jets of high transverse momenta is needed for these channels which is therefore not very sensitive to performance degradations at higher luminosity.

## 9 Searches for excited quarks

Section 21.3 of Ref [1] and Ref. [27] discuss signals for new exotic quarks. Some of these studies have been repeated for the upgrade scenarios. The decays $q^* \to qg$ and $q^* \to q\gamma$ have been simulated. Figures 19 and 20 show the statistical significance of the signal in these channels as a function of the excited quark mass in the $jet-jet$ and $jet-\gamma$ final states. The mass reach increases by about 4 TeV for the highest energy/luminosity configuration. As only jets and photons of the very highest transverse energy are needed in the analysis, this process is rather robust even at the very highest luminosity.

## 10 Triple gauge-boson couplings

The final state $W\gamma \to \ell\nu\gamma$ ($WZ \to \ell\nu\ell\ell$) has been used to probe the couplings $\lambda_\gamma$ and $\Delta\kappa_\gamma$ ( $\lambda_Z$, $\Delta\kappa_Z$ and $g_1^Z$) that describe the $WW\gamma$ ($WWZ$) interaction vertex. More details of the methodology can be found in Section 16.2 of [1]. For a luminosity of $10^{35}$ cm$^{-2}$ sec$^{-1}$, the analysis reported here uses only muons and photons. This represents a loss of 50% (75%) of the $W\gamma$ ($WZ$) effective rate. The constraints on the $\kappa$ couplings arise primarily from the angular distributions whereas those on the $\lambda$ couplings arise from the transverse momentum distributions. As only the latter are used here, the results are pessimistic in the case of the $\kappa$ couplings. The expected sensitivity is shown in Table 10 and the correlations in Fig. 21. Note that both the energy or luminosity upgrades extend the sensitivity for $\lambda_\gamma$ into the range ($\sim 0.001$) expected from radiative corrections in the Standard Model and should allow a meaningful test of these corrections and others that arise for example in supersymmetric models.

In contrast to most of the other examples discussed, the luminosity increase is more powerful than the energy increase in this case.

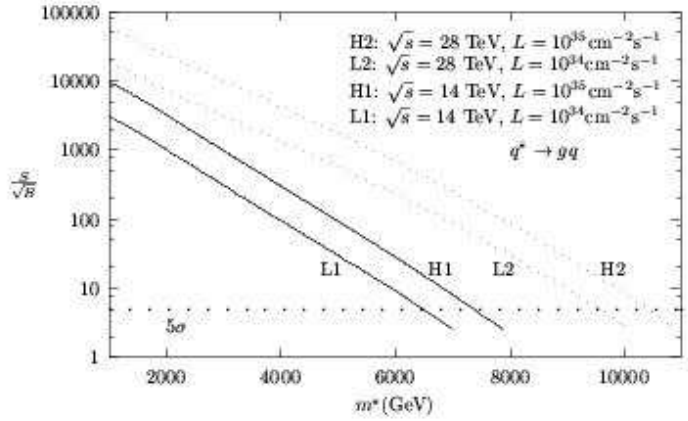


Figure 19: The statistical significance of an excited quark signal as a function of the excited quark mass in the final state $jet + jet$ at 14 and 28 TeV and integrated luminosities of 100 and 1000 fb$^{-1}$.

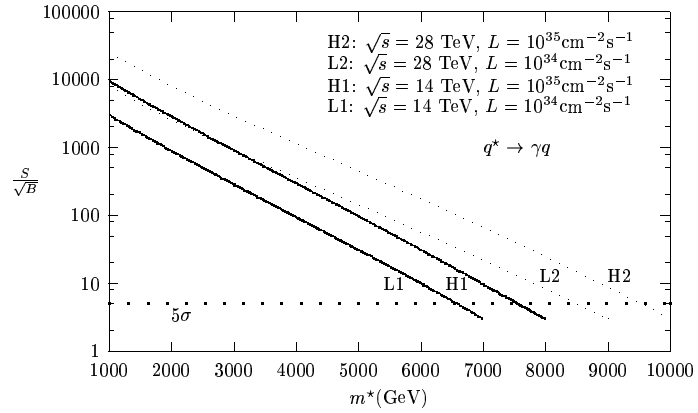


Figure 20: The statistical significance of an excited quark signal as a function of the excited quark mass in the final state $\gamma + jet$ at 14 and 28 TeV and integrated luminosities of 100 and 1000 fb$^{-1}$.

| Coupling | 14 TeV | 14 TeV | 28 TeV | 28 TeV |
|---|---|---|---|---|
| | 100 fb$^{-1}$ | 1000 fb$^{-1}$ | 100 fb$^{-1}$ | 1000 fb$^{-1}$ |
| $\lambda_\gamma$ | 0.0014 | 0.0006 | 0.0008 | 0.0002 |
| $\lambda_Z$ | 0.0028 | 0.0018 | 0.0023 | 0.009 |
| $\Delta\kappa_\gamma$ | 0.034 | 0.020 | 0.027 | 0.013 |
| $\Delta\kappa_Z$ | 0.040 | 0.034 | 0.036 | 0.013 |
| $g_1^Z$ | 0.0038 | 0.0024 | 0.0023 | 0.0007 |

Table 10: 59% C.L. constraints on the triple gauge boson couplings

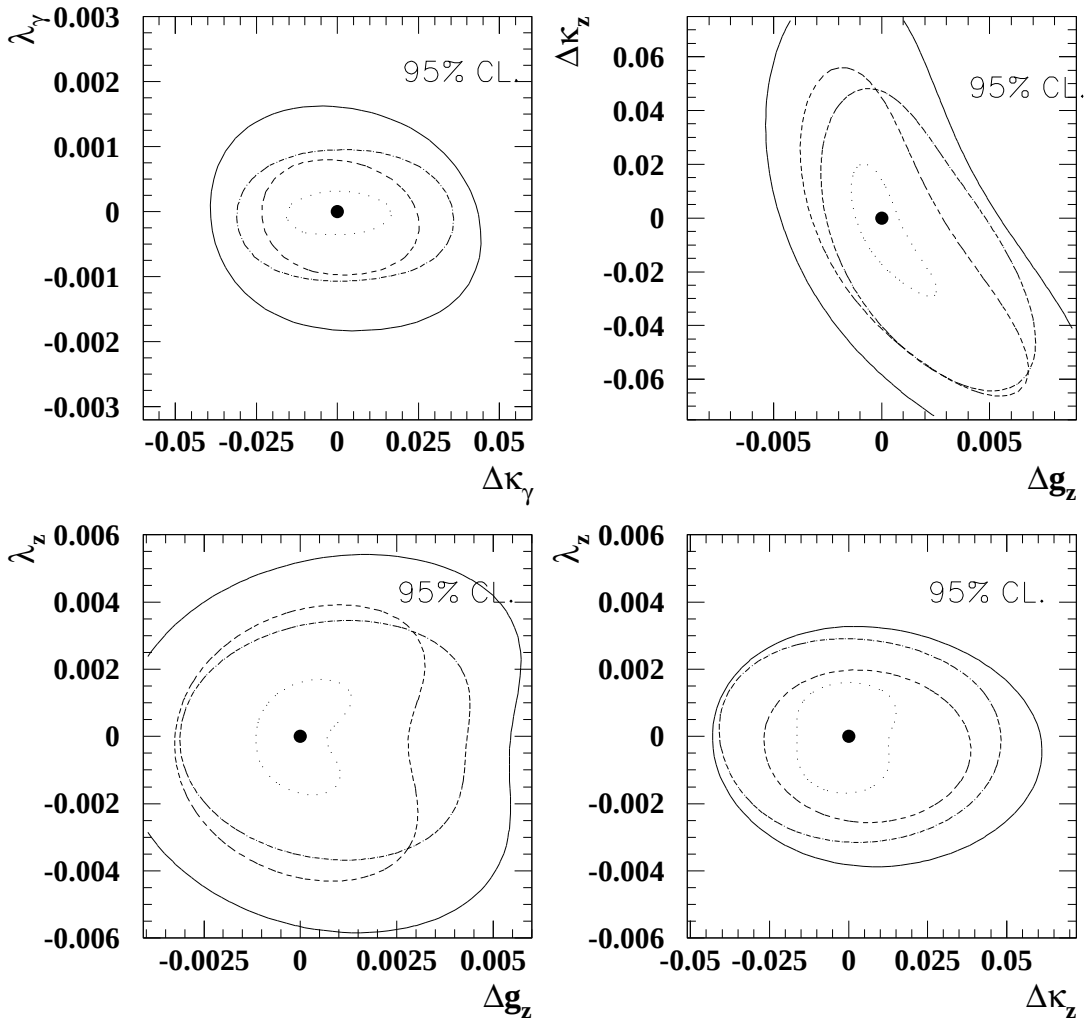


Figure 21: Expected 95% C.L. constraints on triple gauge-boson couplings $\kappa$ and $\lambda$ resulting from two parameter fits. The contours correspond to 14 TeV and 100 fb$^{-1}$ (solid), 28 TeV and 100 fb$^{-1}$ (dot dash), 14 TeV and 1000 fb$^{-1}$ (dash), 28 TeV and 1000 fb$^{-1}$ (dotted).

## 11 Comments and conclusion

Although there are other processes where some impact from the upgrades can be expected and which have not been studied, this survey of physics processes at an upgraded LHC enables one to draw certain conclusions.

Without major detector upgrades, *i.e.* by using only final states of high $p_T$ jets, photons and muons, a luminosity upgrade is expected to provide a $\sim 20\%$ improvement in the mass reach for new physics as SUSY and extra-dimensions. This increase is significant for signals at the limit of the LHC sensitivity. However, the failure of the Inner Detector will compromise electron identification as well as b and hadronic $\tau$ tagging. For many new physics processes, statistical samples are improved by combining channels with electrons and muons. In addition valuable information about new physics can be obtained by looking for violation of $e/\mu/\tau$ universality. Therefore major detector upgrades would be needed to exploit fully the factor of ten increase in luminosity. Pile-up of minimum bias events has severe impact on the ability to use forward jet tagging and central jet vetoing as a tool to enhance signal to background ratios at luminosities significantly higher than $10^{34}$ cm$^{-2}$ sec$^{-1}$.

The energy upgrade would be much easier to exploit. It could significantly enhance the physics reach of the LHC by almost a factor of two in mass. In addition, if new physics is discovered, then the energy upgrade would allow significant further study of the new physics. However, this scenario remains speculative.

## References


[1] ATLAS Collaboration, "ATLAS Physics and Detector Performance Technical Design Report," LHCC 99-14/15 (1999).

[2] W.T. Giele *et al.*, Nucl. Phys B403 (1993) 633.

[3] M. Hohlfeld, Atlas Internal Note, ATL-PHYS-2001-004.

[4] The LEP Electroweak Working Group, CERN-EP-2000-016.

[5] G. W. Anderson and D. J. Castaño, Phys. Rev. **D52**, 1693 (1995) [hep-ph/9412322].

[6] H. N. Brown *et al.* [Muon g-2 Collaboration], Phys. Rev. Lett. **86**, 2227 (2001) [hep-ex/0102017].

[7] A. Czarnecki and W. J. Marciano, hep-ph/0102122.

[8] J. Ellis, D. V. Nanopoulos and K. A. Olive, hep-ph/0102331.

[9] L. L. Everett, G. L. Kane, S. Rigolin and L. Wang, Phys. Rev. Lett. **86**, 3484 (2001) [hep-ph/0102145].

[10] H. Baer, C. Balazs, J. Ferrandis and X. Tata, hep-ph/0103280.

[11] S. P. Martin and J. D. Wells, hep-ph/0103067.

[12] J. L. Feng and K. T. Matchev, Phys. Rev. Lett. **86**, 3480 (2001) [hep-ph/0102146].

[13] L. Alvarez-Gaume, J. Polchinski and M.B. Wise, Nucl. Phys. **B221**, 495 (1983);
L. Ibañez, Phys. Lett. **118B**, 73 (1982);
J.Ellis, D.V. Nanopolous and K. Tamvakis, Phys. Lett. **121B**, 123 (1983);
K. Inoue *et al.* Prog. Theor. Phys. **68**, 927 (1982);
A.H. Chamseddine, R. Arnowitt, and P. Nath, Phys. Rev. Lett., **49**, 970 (1982).

[14] W. Beenakker, R. Hopker and M. Spira, hep-ph/9611232.

[15] H. L. Lai *et al.*, Phys. Rev. **D51**, 4763 (1995) [hep-ph/9410404].

[16] J. Bagger, J. L. Feng and N. Polonsky, Nucl. Phys. B **563**, 3 (1999) [hep-ph/9905292].

[17] J. L. Feng, K. T. Matchev and T. Moroi, Phys. Rev. Lett. **84**, 2322 (2000) [hep-ph/9908309].

[18] H. Baer, C. Balazs, P. Mercadante, X. Tata and Y. Wang, hep-ph/0008061 (2000).

[19] F. Paige and S. Protopopescu, in *Supercollider Physics*, p. 41, ed. D. Soper (World Scientific, 1986);
H. Baer, F. Paige, S. Protopopescu and X. Tata, in *Proceedings of the Workshop on Physics at Current Accelerators and Supercolliders*, ed. J. Hewett, A. White and D. Zeppenfeld, (Argonne National Laboratory, 1993).

[20] E. Richter-Was, D. Froidevaux and L. Poggioli, Atlas Internal Note ATL-PHYS-98-131 (1998).

[21] ATLAS Liquid Argon Calorimeter Technical Design Report, CERN/LHCC/96-41 (1996)

[22] M. S. Chanowitz and M. K. Gaillard, Nucl. Phys. **B261** (1985) 379.

[23] A. Dobado, M. J. Hererro, J. R. Pelaez and E. Ruiz Morales, Phys. Rev. **D62** (2000) 055011
S. Haywood *et al.*, in *Proceedings of the Workshop on Standard Model (and more) at the LHC, Chapt. 3: Electroweak Physics*, CERN-2000-004 (2000).

[24] A. Pukhov *et al.*, COMPHEP - a package for evaluation of Feynman Diagrams and Integration of Multi-particle Phase Space, INP MSU 98-41/542 (hep-ph/9908288).

[25] J. A. Bagger *et al.*, Phys. Rev. **D52** (1995) 3878.

[26] L. Vacavant and I. Hinchliffe, hep-ex/0005033 (2000).

[27] O.Cakir, R.Mehdiyev, Phys. Rev., **D60**, 034004 (1999); O. Cakir, C. Leroy and R. Mehdiyev, Phys. Rev. D **62**, 114018 (2000), **63**, 09414 (2001).